Drone Systems and Applications

OPEN ACCESS | Article

Validation of wind measurements from a multirotor RPAS-mounted ultrasonic wind sensor using a ground-based LiDAR system

Leo Scicluna [a], **Tonio Sant** [a], **and Robert N. Farrugia** [b]

[a]Department of Mechanical Engineering, University of Malta, Msida, MSD 2080, Malta; [b]Institute for Sustainable Energy, University of Malta, Marsaxlokk, MXK 1531, Malta

Corresponding author: **Leo Scicluna** (email: leo.scicluna.99@um.edu.mt)

Abstract

The aim of this research was to establish the validity of wind measurements from on board a multirotor Remotely Piloted Aircraft System (RPAS) for the purposes of wind monitoring applications. A custom-built hexacopter RPAS recorded wind speed and direction by means of an onboard ultrasonic wind sensor, whilst operating in the inherently highly stochastic nature of open field atmospheric conditions. Experimental data were collected during open field hovering flights subject to different ambient conditions with free stream horizontal wind speeds reaching up to 12 m/s. Flights were conducted at different altitudes above ground level and in proximity to a Light Detection and Ranging (LiDAR) remote wind measurement unit that was used as a low-resolution reference meteorological station. Very good correlation was obtained between the RPAS and LiDAR unit for both wind speed and wind direction measurements across all hovering flight altitudes. The RPAS-based wind speed measurements were found to have a consistent 1 m/s positive offset, whilst the RPAS-based wind direction readings had a 6.16° negative offset. These were potentially caused by differences in the localized wind fields between the LiDAR and RPAS measuring positions, as well as by localized RPAS rotor-induced air flows for wind speed measurements and potential slight misalignments in the instruments' reference datum for wind direction readings.

Key words: hexacopter, multirotor, remotely piloted aircraft system (RPAS), unoccupied aerial vehicles (UAVs), wind measurement

1. Introduction

Over the past decades the use of Remotely Piloted Aircraft Systems (RPASs) and micro aerial vehicles has increased substantially, whilst the areas of deployment for such vehicles have diversified extensively. Amongst the different sectors in which RPASs are being deployed, one may find environmental surveying, mapping and monitoring (Drummond et al. 2015), logistics (FedEx Newsroom 2019; CNBC 2020; DHL 2020), as well as in search and rescue operations (Read 2017) in aiding first responders in the aftermath of natural disasters (Estrada and Ndomab 2019). Applications for the purposes of emergency delivery of life-saving goods such as blood products (Amukele et al. 2017) and devices such as life rings for individuals in difficulty at sea (Xiang et al. 2016) are also being studied. RPASs are also rapidly gaining popularity in the fields of remote inspection of various structures (Eschmann et al. 2012; Hallermann and Morgenthal 2013; Tyutyundzhiev et al. 2015), whilst deployment of RPASs for the purposes of wind monitoring applications and wind turbine inspections at wind farm sites is also on the rise with several organizations already offering such services on a commercial basis (Willis et al. 2018; Aerialtronics 2020; Iberdrola 2020).

Whilst weather balloons are more adapted to obtain measurements for vertical wind profiling, it is much more challenging to take weather measurements at a fixed location in space for an established duration of time using balloon technology, as they are relatively uncontrolled devices, dependent on the wind conditions at the time of flight and at the altitude attained. Meteorological masts and towers are also commonly used, especially when continuous measurements over an extended period are required. Nonetheless, these become less cost-effective when measurements at multiple locations and at increasingly higher altitudes are required.

RPASs and associated onboard measuring technologies offer substantial benefits for wind monitoring and wind turbine wake profiling operations. Multirotor RPASs offer a stable platform for the mounting of measuring equipment, whilst being capable of maintaining a stable hover at a fixed point in 3D space with unparalleled flexibility for the purposes of measurement site selection. These advantages are more fully appreciated when wind monitoring operations are conducted at remote locations usually having limited accessibility, such as remotely located onshore wind farm sites and to a greater extent at offshore wind turbine installations

occasionally located at a substantial distance from the nearest coastline. Furthermore, RPAS operations may be easily launched from the relative safety of a vessel at sea, with the possibility of conducting such measurements even in less-than-ideal weather conditions.

The uptake of such RPAS technologies in the wind monitoring sector is further driven by the continuous improvements in performance and capabilities of RPASs, with atmospheric data sensors specifically developed for mounting onto RPAS platforms (Anemoment 2018; FT Technologies 2019; InterMet Systems 2020). Nonetheless, the deployment of such mobile platforms for wind data measurements may give rise to measurement uncertainties, mainly due to RPAS motion during the data collection window, which could in turn influence the validity of the onboard wind sensor's measured data.

This new research addresses these operational uncertainties by evaluating the viability of an RPAS-mounted wind sensor as an accurate means of wind measurement. The methodology involves comparing open field measurements using an RPAS-mounted ultrasonic wind sensor against those obtained by a ground-based Light Detection and Ranging (LiDAR) wind measurement system. This strives to establish whether a multirotor RPAS-mounted wind sensor can be utilized in lieu of accepted ground-fixed conventional methods of measuring atmospheric wind data; albeit for short durations given the current RPAS time of flight limitations. The overarching objective being to provide key information to support the eventual development of airborne vehicles for the accurate measurement of atmospheric parameters, such as wind speed and direction, as a complimentary platform to currently established ground-based wind measuring systems.

1.1. Current research

Abichandani et al. (2020) provide an extensive review of the various RPAS-based techniques used for the purposes of wind measurement or estimation as well as simulation modelling techniques for such platforms. Meier et al. (2022) propose a dynamic model-based approach utilizing the thrust generated by a multirotor RPAS to estimate the wind. In a study by Gonzalez-Rocha et al. (2020), the authors obtain model-based wind velocity estimates using a rigid body model. It was established that wind velocity model-based estimates from quadcopter motion may also be obtained for steady ascent flight speeds of up to 2 m/s; however, it was highlighted that the accuracy of the model-based wind estimates is highly dependent on the motion model accuracy.

Nolan et al. (2018) conducted a study using two RPASs equipped with ultrasonic anemometers at altitudes of up to 15 m above ground level. For a typical calibration flight, which formed part of a wider study, the authors reported a root mean square error (RMSE) of 0.75 m/s and 8.9° for wind speed and direction, respectively, when the RPAS-based measurements were compared to ground-based instruments.

Wolf et al. (2017) explored different methods for obtaining wind data using a quadcopter platform by carrying out tests in an indoor simulated wind environment, including the use of different types of onboard anemometers and the use of RPAS parameters for wind estimation purposes. Marino et al. (2015) conducted a quadcopter RPAS viability study under wind tunnel conditions and examined the possibility of using such vehicles for wind data sensing around tall buildings. In another study, Prudden et al. (2018) demonstrated how the wind velocity and turbulence intensity, captured by an airborne platform such as a quadcopter using a multihole pressure probe, were feasible.

Nonetheless, the acceptance by meteorologists of wind data measured with an RPAS-mounted wind sensor is dependent on the confidence level of such wind data in comparison with wind measurements collected using accepted "conventional" means. Studies comparing measurements from a hexacopter RPAS-mounted ultrasonic anemometer to wind data from propeller-vane anemometers mounted on a meteorological mast at heights of 40 and 55 m above ground level (Shimura et al. 2018) and to a 3D sonic anemometer at an altitude of 10 m above ground (Palomaki et al. 2017) were conducted. The former study was limited to five RPAS flights with a range of open field wind speeds of up to 11 m/s, whilst the latter was conducted in light to moderate wind speeds of up to 5 m/s. Both studies found a wind speed bias of 0.5 m/s for the RPAS-mounted sensor, with the latter study also reporting occasional overestimations of the wind speed of 1 m/s. In another study by Thielicke et al. (2021) using a quadrotor-mounted ultrasonic anemometer, the authors also reported a wind speed bias in the RPAS-mounted sensor readings, both during wind tunnel tests and when operating in close proximity to a bistatic LiDAR. Shimura et al. (2018) also compared RPAS-based wind measurements with two wind data sets from Doppler LiDARs situated at relatively distant locations (4 and 5 km) from the RPAS operations site for the purposes of wind vector profiling up to an altitude of 1000 m above ground level.

1.2. Project definition

The main findings in the literature available to date on the reliability of measurements obtained using multirotor RPASs may be consolidated as follows:

1. Most studies used data measured by conventional wind sensors mounted on meteorological masts at a relatively low altitude near the test site being used as reference. One study compared RPAS data to those from LiDAR units which were located at a large distance (>1 km) away from the RPAS flight site.
2. Ultrasonic wind sensors emerge as the preferred sensor type for wind monitoring applications using a multirotor RPAS.
3. Wind speed measurements acquired by RPAS-mounted wind sensors are commonly logged at a frequency of 1 Hz (Palomaki et al. 2017; Shimura et al. 2018). In general, such measurements have a positive wind speed bias in the range of 0.5 m/s (Shimura et al. 2018) to 1 m/s (Palomaki et al. 2017). As for the measured wind direction, studies seemingly indicate that such readings remain relatively unaffected.

Fig. 1. The completed hexacopter RPAS setup.

It transpires that wind correlation studies conducted to date have been wind tunnel-based or carried out in other indoor controlled environments, whilst open field studies were conducted at relatively low altitudes and under low, open field wind speeds, whilst also being restricted to a limited number of flights.

It was thus established that an extensive wind correlation study of wind measurements taken by an RPAS-mounted wind sensor operated at different altitudes above the ground and covering a wide range of wind speeds, was necessary, to further establish an acceptable level of confidence in measurements obtained from such RPAS-mounted anemometers. The current study addresses this research gap by conducting an extensive analysis of hexacopter RPAS-based ultrasonic sensor wind measurements, covering a free stream wind speed range of up to 12 m/s. These measurements were collected in open field conditions and in close proximity to a low-resolution reference LiDAR wind measurement unit for a range of altitudes between 40 and 100 m above the LiDAR unit's reference window. The wind measurements logged by the two instruments were then used to carry out a detailed correlation analysis of wind speed and wind direction.

This paper is organized as follows: An overview of the multirotor RPAS developed specifically for this study is given in Section 2, followed by the methodology employed for collecting the necessary data sets in Section 3. Section 4 details the results obtained, which is then followed by a discussion of the key results in Section 5. The main findings and conclusions, together with potential areas of further research identified during this study, are outlined in Section 6.

2. Development of a multirotor RPAS design

Since this study focused on wind monitoring applications employing hovering RPASs, the multirotor RPAS platform of the hexacopter type was chosen as a test vehicle because of its ability to maintain a steady hover, and its capability of remaining airborne in the event of loss of one rotor, making this type of RPAS safer to operate.

The multirotor RPAS consisted of two main systems. Although the two systems were physically integrated into one vehicle, as shown in Fig. 1, these were considered as two separate units for development purposes, namely,

1. the multirotor platform, and
2. the sensor suite.

2.1. The multirotor platform

The chosen hexacopter frame was a modified off-the-shelf Tarot FY680 frame (Tarot-Rc 2020), made of lightweight carbon fibre-reinforced polymer (CFRP) and aluminium alloy fittings.

A new battery mount was specifically developed to install the RPAS battery to the underside of the RPAS platform, whilst the original battery mounting plate on top of the RPAS frame was modified and fitted with a baseplate for a CFRP vertical pole onto which the ultrasonic wind sensor was mounted (Fig. 1). This setup also improved the weight distribution of the RPAS about its vertical axis geometric centre, and consequently improved stability during flight.

Fig. 2. The ZephIR ZX 300 LiDAR unit installed on the rooftop of a building, at Ċirkewwa, l/o Mellieħa, Malta.

The original pair of landing skids of the Tarot FY680 hexacopter frame were modified to a 500 mm × 500 mm square footprint, increasing the RPAS's stability during the landing phase and hence minimizing the potential of tipping over during landing, especially in windy conditions (Fig. 1).

The propulsion arms of the hexacopter frame were fitted with motor mounts intended for the Tarot 680 Pro model. This resulted in an increased rotor-to-rotor diagonal distance of 805 mm which enabled the DJI 1345 propellers to fit properly on the hexacopter frame.

The flight controller used for the developed multirotor platform was a DJI N3 unit, which also had a data logging function for various flight parameters (DJI 2017), whilst a DJI E800 tuned propulsion system (DJI 2015) was used for the propulsion of the RPAS multirotor. The DJI 3510 motors used were 350 rpm/V Brushless Direct Current motors of the out-runner type. These were individually driven by an E-series 620S Electronic Speed Controller (ESC). The propellers fitted onto the out-runner motors were DJI 1345 twin-bladed fixed pitch propellers, having a diameter of 345 mm (13.6 in.) and a pitch of 115 mm (4.5 in.), with each of the propeller-motor-ESC assemblies having a maximum thrust capability of 2100 g at a supply voltage of 25 V at sea level.

2.2. The sensor suite

The sensor suite measured and logged the wind speed and direction as measured by the onboard ultrasonic wind sensor.

2.2.1. The ultrasonic wind sensor

The FT205EV ultrasonic wind sensor specifically developed for RPAS applications by FT Technologies (FT Technologies 2019) was selected for the wind speed and wind direction measurements. The sensor, which has a resolution of 0.1 m/s and an of accuracy ± 0.3 m/s for wind speed and a resolution of 1° and an accuracy of 4° RMS for wind direction, was mounted atop a 500 mm pole fitted above the RPAS's centre hub to minimize the potential effect of the RPAS rotor-induced airflow on the free stream conditions. The FT205EV ultrasonic wind sensor was selected based on its overall weight of 100 g and minimal aerodynamic profile – two very important characteristics, which have a substantial impact on the RPAS's stability and tolerance to high winds.

2.2.2. An Arduino-based data logger

An Arduino Mega 2560 Rev 3 development board was used to assemble an independent data logging system specifically developed to log wind data from the FT205EV wind sensor. A Global Positioning System (GPS) data logger shield incorporating a NEO-6M GPS receiver and a microSD card writer was stacked onto the Arduino Mega 2560 Rev 3 board. Each FT205EV wind sensor measurement was GPS timestamped and written to the microSD card at a frequency of 5 Hz.

2.3. The LiDAR wind measurement unit

Wind measurements collected from the RPAS in flight were compared to a reliable data set collected concurrently at the same test site using a ZephIR ZX 300 LiDAR wind measurement unit (ZXLidars 2020). This ground-based LiDAR unit is a continuous wave LiDAR system wind measurement instrument with a capability of measuring wind speed and direction at 10 different pre-set altitudes above the measurement window. The instrument was installed on the rooftop of the

Fig. 3. RPAS operations site at Ċirkewwa, l/o Mellieħa, Malta. Also shown is Aħrax Point (Satellite imagery: Google Earth 2020).

Water Services Corporation's Reverse Osmosis (RO) plant at Ċirkewwa, l/o Mellieħa, Malta (Fig. 2). The coordinates for its installed position were 35.98596°N, 14.33514°E, and the measurement window of the unit was set at 6 m above street level. The ZephIR ZX 300 LiDAR unit measured wind speed and wind direction at accuracies of ± 0.1 m/s and a direction variation of less than 0.5°, respectively.

3. Data collection methodology

This section gives an overview of the data collection methodology adopted throughout this study. Several sites were identified for the different stages of this study. Operational sites were identified for

1. Open Field Data Collection Flights,
2. Sheltered Data Collection Flights, and
3. Tied-Down Data Collection Tests.

3.1. Site for open field data collection flights

The Maltese islands consist of a small archipelago located in the central Mediterranean basin. The prevailing wind direction over the Maltese islands is the *Majjistral* (north-west), as clearly indicated in a long-term climate report for the Maltese islands by Galdies (2011) and in studies conducted by Farrugia and Sant (2011) for a site at Wied Rini, as well as at Aħrax Point (Farrugia and Sant 2016). The Aħrax Point site for the latter study lies approximately 3 km to the east-north-east of the location chosen for the RPAS operations in connection with the current study, as indicated in Fig. 3.

It was desired that the wind conditions at which the RPAS data collection flights were conducted would have a low turbulence intensity (<10%). A coastal location at Ċirkewwa, l/o Mellieħa, at the northwestern tip of the island of Malta that is well exposed to relatively unobstructed wind flows from the northwesterly winds was thus selected. It was also considered necessary that the selected hover site for the open field data collection flights was such that the operating RPAS and the RPAS rotors' induced airflows did not disturb the LiDAR wind measurement unit's readings. The hover site for the data collection flights was thus chosen to be downwind of the LiDAR wind measurement unit when subjected to the prevailing *Majjistral* winds (Fig. 4). This site was retained for all data collection flights throughout the measurement campaign, independent of the wind direction at the time of each flight.

3.2. Site for sheltered location data collection flights

Flights were also conducted in the courtyard of a building in the town of Qormi having a highly symmetrical octagonal shape measuring 17.5 m diagonally. The intention of this set of flights was to eliminate external influences on the RPAS which was shielded from atmospheric air currents by the building's 9 m high surrounding walls.

3.3. Site for tied-down testing

The sheltered location flights were complemented by a set of RPAS tied-down tests, both of which were intended to establish whether the readings of the RPAS-mounted ultrasonic wind sensor were biased by the localized flow field induced by the RPAS rotors. Since these tests were ground-based, these tests also included the logging of wind data with the RPAS in powered down mode, and hence with no consequent rotor influence. These tests were carried out in a sheltered open space measuring approximately 6.5 m × 6.5 m square, protected by a 1 m high boundary wall on the southern and eastern sides, and 3 and 7 m high walls on the northern and western sides, respectively.

Fig. 4. Aerial image of the Ċirkewwa RPAS operations site showing the diameter of the LiDAR unit measuring cone at the RPAS hovering altitudes, in relation to the RPAS data collection hover site (Satellite imagery: Google Earth 2020).

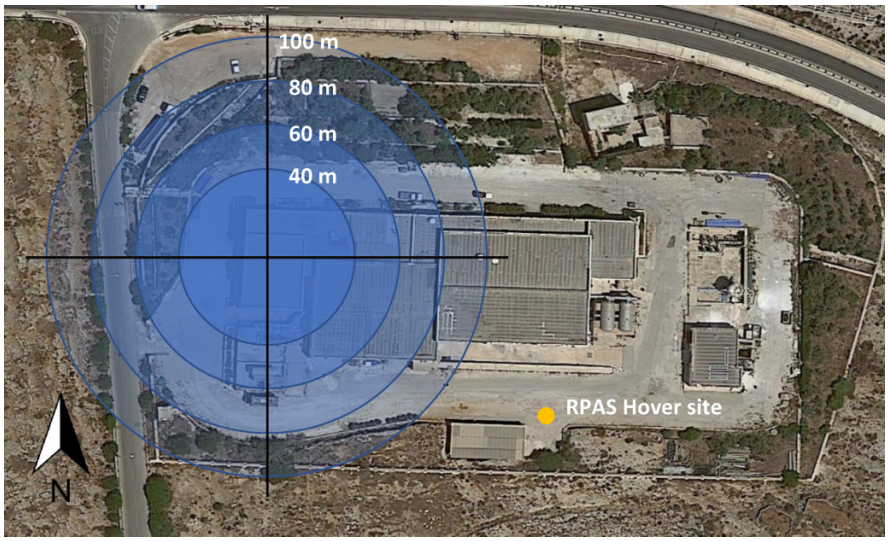

3.4. RPAS data collection flights

To maximize the number of data points for use in the respective correlation analysis, 40 data collection flights were conducted from the Ċirkewwa site between December 2019 and March 2020. The RPAS was operated approximately 75 m southeast of the LiDAR site, as graphically shown in Fig. 4. The flights were conducted at four different altitudes, namely 40, 60, 80, and 100 m above the LiDAR's measurement window and thus coincident with heights at which LiDAR wind measurements were being concurrently measured and logged. Open field data collection with the hexacopter RPAS was conducted at a fixed RPAS heading with a minimum uninterrupted data collection time of 5 min in hover.

Following the data collection campaign at the Ċirkewwa site, control flights were conducted at an altitude of 5 m above ground level to minimize any ground effect phenomena, in the detailed sheltered location between May 2020 and July 2020, whilst tied-down tests were executed at the detailed test site with the RPAS tied down to a rig with its rotors sitting 1.2 m (equivalent to 3.5 rotor diameters) above the ground.

4. Results and analysis

The data collected during the data collection flights were post-processed. The wind direction readings recorded by both instruments were adjusted with respect to True Geographical North using declination values obtained from the International Geomagnetic Reference Field model (National Oceanic and Atmospheric Administration 2020). Furthermore, the wind measurements recorded by the two instruments were synchronized using the respective GPS timestamps of each of the logged records. A standard least squares approach was adopted for the regression analyses pertaining to the wind correlation studies for both the wind speed and wind direction data sets.

4.1. Incident wind during flight operations

The ground-based LiDAR remote wind measurement unit logged wind data continuously, whilst the multirotor RPAS-mounted ultrasonic wind sensor logged wind data whilst the aircraft was in flight. Wind rose plots of the incident horizontal wind speed and direction as measured by the ultrasonic wind sensor during the execution of the hexacopter RPAS data collection flights are shown in Fig. 5.

Due to the different nature of the two instruments, the wind data from each unit were logged at a different frequency. At each pre-set measurement height, the ZX 300 LiDAR scanned the circumference of a full 360° disk through the air, collecting 50 samples from around the scanned disk at equally spaced intervals every 20 ms. The values collected for every scan were then averaged by the unit to output a 1 s average at the specified measurement height. This resulted in a unit output of approximately three 1 s average readings of wind speed and direction for every pre-set altitude per minute, resulting in a sampling period of approximately 20 s. Contemporarily, the ultrasonic wind sensor logged data at a consistent frequency of 5 Hz. Due to the substantial discrepancy between the logging frequencies, it was impractical to study the correlation between individual wind data readings. In view of this, each LiDAR reading was compared to the average of the corresponding logged data from the ultrasonic wind sensor over the time interval between the concurrent LiDAR reading and the preceding reading. This resulted in a total of 573 data points across all hovering altitudes for an equivalent RPAS hover time of approximately 4 h.

The wind direction averaging computation was weighted with the respective wind speeds using eq. 1. This led to the value of wind direction computed over the averaging range to be the equivalent of the wind direction at the averaged wind speed.

$$\bar{\theta} = \arctan\left(\sum_{i=1}^{N} V_{\infty i}\sin\theta_i \Big/ \sum_{i=1}^{N} V_{\infty i}\cos\theta_i\right) \quad (1)$$

Fig. 5. Wind rose plots for incident horizontal wind with respect to true north as measured by the hexacopter RPAS-mounted ultrasonic wind sensor during hover operations.

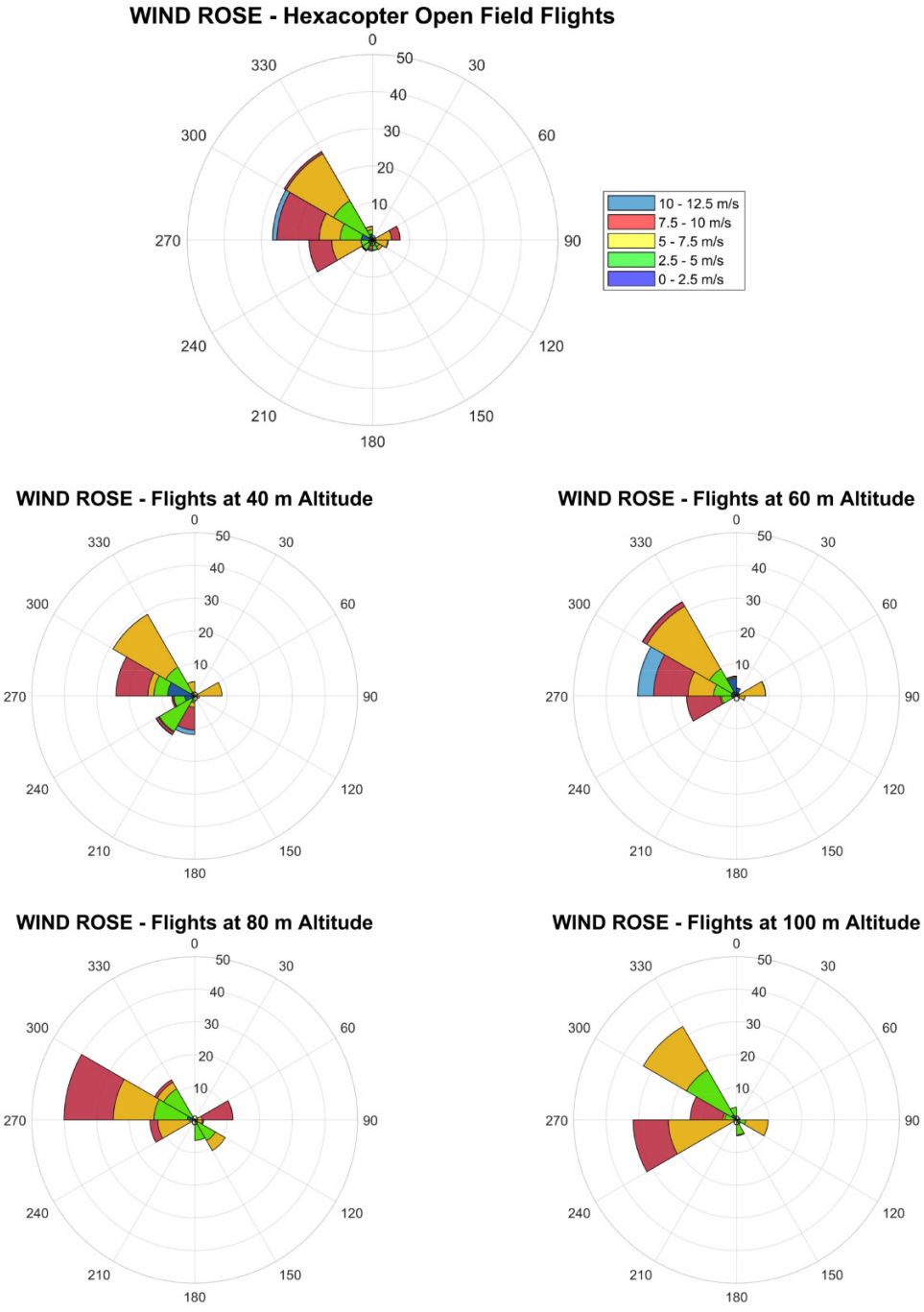

where θ is the wind direction in degrees and V_∞ is the wind speed in m/s.

4.2. Wind measurement correlations

To establish whether the wind data measured and collected by the RPAS-mounted wind sensor can be reliably considered as a true measure of the actual wind conditions at the location of the sensor, plots of the wind speed, and the respective wind direction from both the LiDAR measurements and the onboard ultrasonic wind sensor were prepared.

4.2.1. Wind speed correlation

A plot for the wind speeds measured by the RPAS-mounted ultrasonic wind sensor with respect to the LiDAR wind measurement unit readings for wind speed is shown in Fig. 6 for data across all hovering altitudes. The plot indicates that there exists a relatively strong correlation between the two independently logged data sets, as indicated by the R^2 value shown in the accompanying table.

The strong wind speed correlation was found to be consistent across the four data sets segregated by the different flight

Fig. 6. Hexacopter RPAS-mounted ultrasonic sensor wind speed readings with respect to LiDAR wind speed readings.

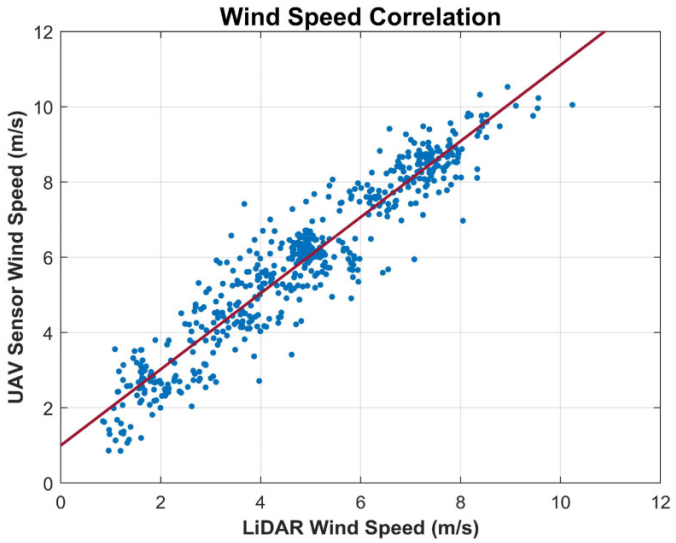

Data set	Model	No. of Data Points	R^2	RMSE *(m/s)*
All	$V_{UAV} = 1.01V_{LID} + 1.00$	573	0.896	0.702

altitudes at which wind speed measurements were taken, as demonstrated in the plots for records segregated by flight altitude (Fig. 7).

4.2.2. Wind direction correlation

Similar to the wind speed correlation analysis, the correlation strength between the wind direction readings from the two independent instruments was established by a plot for the ultrasonic sensor wind direction readings with respect to LiDAR wind direction readings. This is shown in Fig. 8 for data across all hovering altitudes. A series of plots for wind direction data segregated by hovering altitude was also prepared. These indicated that the evident and consistent correlation found in the wind speed data from the two instruments is also present in the wind direction data across the four different hovering altitudes at which data were collected, as demonstrated by the consistently high R^2 values shown in Fig. 9.

It is interesting to observe that for both wind speed and wind direction correlation analyses, the RMSE decreases progressively as the altitude increases. This is indicative of an increasingly homogeneous wind flow field as the altitude increases, potentially due to the decreasing influence of the different ground topographies between the LiDAR site and the RPAS hovering site.

Having established the correlation between the wind direction recorded by the LiDAR wind measurement unit and the hexacopter RPAS-mounted ultrasonic wind sensor, it was interesting to analyse whether the correlation was consistent across the full range of wind speeds. The wind direction delta, which is the difference in the values of wind direction recorded by the RPAS-mounted ultrasonic wind sensor and the LiDAR wind measurement unit was calculated for each corresponding pair of wind direction readings. A plot of wind direction delta as the wind speed increases (Fig. 10) indicates that as the wind speed increases, the wind direction readings of the two measuring instruments align closer to each other.

The wind speed correlation analysis revealed that the ultrasonic wind sensor readings are characterized by a positive bias. A minor discrepancy between the wind direction readings of the two instruments is also observed. The ideal method to establish whether the discrepancies in instrument readings were partially or fully caused by the RPAS rotor-induced airflow would have been to fly the RPAS indoors in stable hover. Although this approach was indeed attempted, it was found that this was not a viable solution due to the lack of a GPS signal reception by the RPAS. An attempt to identify this bias was therefore made by making use of sheltered locations for the RPAS flights, as well as by running the RPAS under tied-down conditions. In both scenarios, tests were conducted on relatively windless days to minimize, as much as possible, the influence of any external airflows on these bias identification tests.

4.3. Sheltered location testing

Wind rose plots for wind data measured by the RPAS-mounted ultrasonic wind sensor during the sheltered location data collection flights, for all flights and segregated by individual flights, are presented in Fig. 11. It is apparent that the onboard ultrasonic wind sensor did indeed record an airflow during the course of each flight, although the lack of consistency in the wind direction between flights suggests that the recorded wind data may not be fully attributed to the rotor-induced airflow. Had this been the case, then a consistent wind direction would be expected. Potentially, the

Fig. 7. Hexacopter RPAS-mounted ultrasonic sensor wind speed readings with respect to LiDAR wind speed readings, segregated by operational altitude in hovering flight.

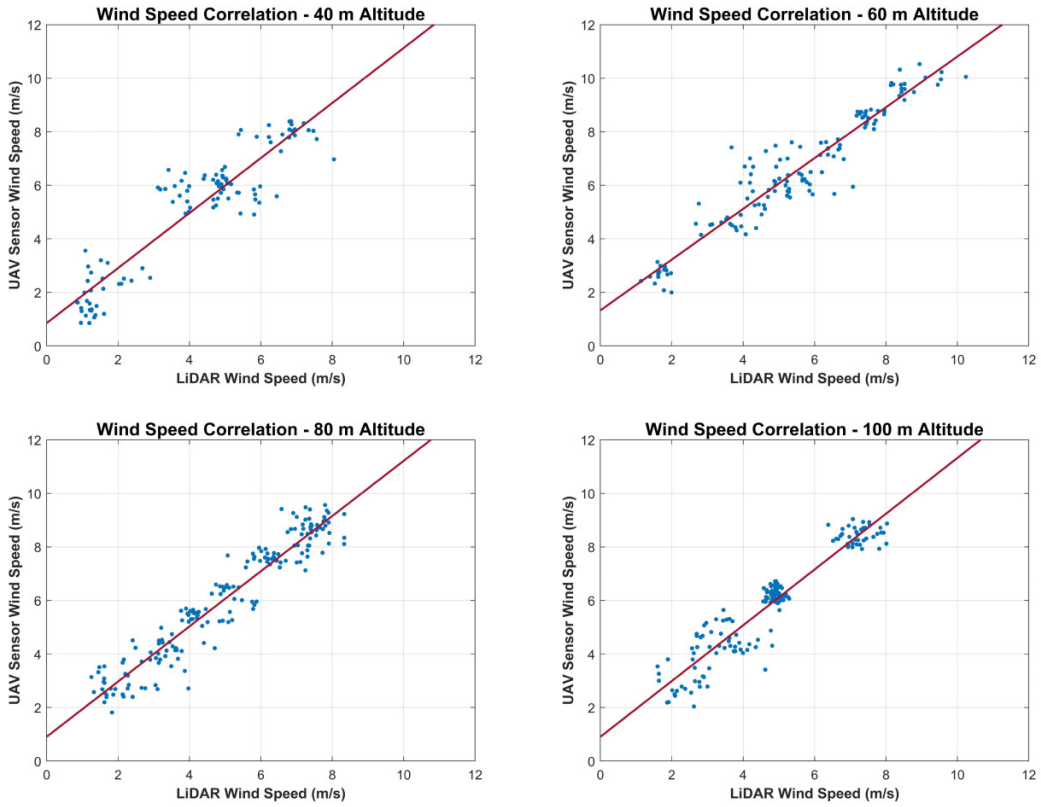

Data set	Model	No. of Data Points	R^2	RMSE *(m/s)*
40 m	$V_{UAV} = 1.03V_{LID} + 0.85$	105	0.852	0.890
60 m	$V_{UAV} = 0.95V_{LID} + 1.33$	134	0.907	0.677
80 m	$V_{UAV} = 1.03V_{LID} + 0.91$	176	0.912	0.657
100 m	$V_{UAV} = 1.04V_{LID} + 0.90$	158	0.892	0.623

recorded values of wind data may be partially due to the presence of incident atmospheric wind flows. On the other hand, the mean recorded wind speed for each individual sheltered flight is relatively consistent as shown in Table 1.

4.4. Tied-down testing

Testing the RPAS under tied-down conditions potentially exposes the RPAS-mounted ultrasonic wind sensor to the most extreme rotor-induced airflow, as the rotors operate at almost maximum power. The configuration of each trial carried out in the tied-down test sequence is described hereunder.

- ***Test 1*** – The RPAS was powered up and the rotors were operated at full power.
- ***Test 2*** – Test conducted with rotor 3, coincident with an RPAS bearing of 270° (see Fig. 12), disconnected, such that an airflow imbalance was created around the ultrasonic wind sensor.
- ***Test 3*** – The RPAS ultrasonic wind sensor was powered up and data for a 3-min interval were logged with the rotors powered down to establish the wind conditions at the time.
- ***Test 4*** – Test conducted with adjacent rotors 3 and 4, coincident with RPAS bearings 270° and 210°, respectively (see Fig. 12), disconnected, with the intention of generating a stronger airflow imbalance.
- ***Test 5*** – The RPAS ultrasonic wind sensor was powered up and data for a second 3-min interval for the wind conditions at the time were recorded, with all rotors powered down.

The data recorded during the two 3-min intervals with the RPAS rotors powered down (Fig. 13) indicate that the wind speed is relatively consistent, whilst the wind direction profile was different when comparing both tests.

Fig. 8. Hexacopter RPAS-mounted ultrasonic sensor wind direction readings with respect to LiDAR wind direction readings.

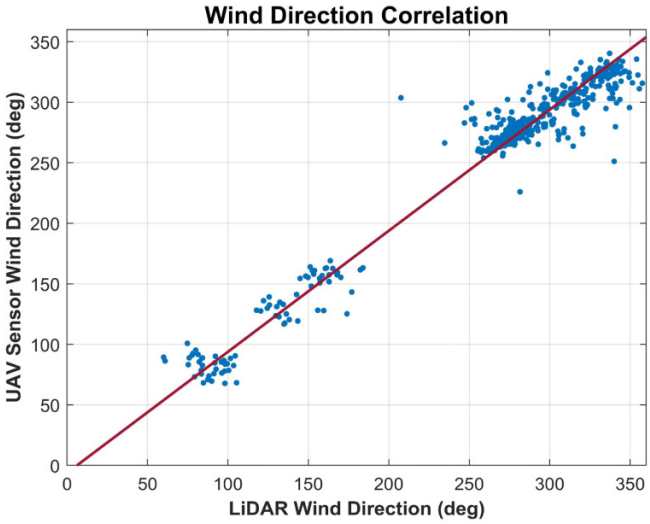

Data set	Model	No. of Data Points	R^2	RMSE (°)
All	$\theta_{UAV} = \theta_{LID} - 6.16$	573	0.951	14.19

When comparing the wind rose plots in Fig. 13 for RPAS tests with powered down rotors with those in Fig. 14 for RPAS tests with rotors powered up, the recorded wind speed was evidently higher when the RPAS rotors were powered up. This indicates that the induced airflow of the RPAS rotors does indeed influence the mounted wind sensor measurements when the RPAS is in close proximity to the ground. From Table 2, the mean recorded wind speed with the RPAS powered down was approximately 0.5 m/s, whilst the mean recorded wind speed with spinning rotors was closer to 2 m/s.

There is also an initial indication that as more rotors are disconnected, the wind speed bias also decreases. Extra caution should be exercised in interpreting this observation as the available data are limited to just three instances, thereby demanding a more detailed analysis based on extended testing and data collection.

Although the rose plots for tests with rotors powered up indicated occasional wind speed readings of 6 m/s or above, these occurrences were minimal (0.66% of the readings recorded with powered up rotors). These were potentially caused by occasional atmospheric breezes interfering with the rotor-induced airflow due to the tests being conducted outdoors. Furthermore, these readings were sampled at a frequency of 5 Hz and, unlike the open field readings were not averaged over a longer time interval, consequently resulting in the smoothing of any open field wind measurement spikes.

While analysing the wind directions recorded during these test flights, it was noticed that the recorded wind direction did not align with the powered down rotors. Incidentally, the wind direction profiles for Test 2 and Test 3, which were executed in rapid succession, seemed to be substantially similar. This similarity, although potentially coincidental, indicates that the wind direction may have been affected by the atmospheric conditions at the time.

It was expected that in Test 2, more occurrences with a wind direction of approximately 270°, and in Test 4, more occurrences of approximately 240° (midway between 210° and 270°), would have been recorded. The lack of proper alignment with the powered down rotors may further indicate that the recorded wind direction may still have been influenced by atmospheric wind conditions at the time of the tests.

Based on the above analyses, it may be claimed that the wind speed recorded by the onboard ultrasonic wind sensor does indeed possess a bias caused by the RPAS's rotor-induced airflow when in close proximity to the ground. Nonetheless, it is considered that further research and dedicated testing are necessary to accurately quantify such a bias under different flight conditions. On the other hand, indications are that the recorded wind direction may be less affected by the potential airflow imbalance, and more dependent on the incident atmospheric wind direction.

5. Discussion

As previously explained in Section 3.1, the selected hovering location was downwind of the LiDAR unit (with respect to the prevalent NW winds). A strategy which potentially gives rise to differences in localized wind fields between the RPAS operations site and the LiDAR's scanning cone, potentially resulting in slight discrepancies in the measured readings. This effect was also attributed to the discrepancies in the readings observed by Shimura et al. (2018) in their wind correlation study.

Fig. 9. Hexacopter RPAS-mounted ultrasonic sensor wind direction readings with respect to LiDAR wind direction readings, segregated by operational altitude in hovering flight.

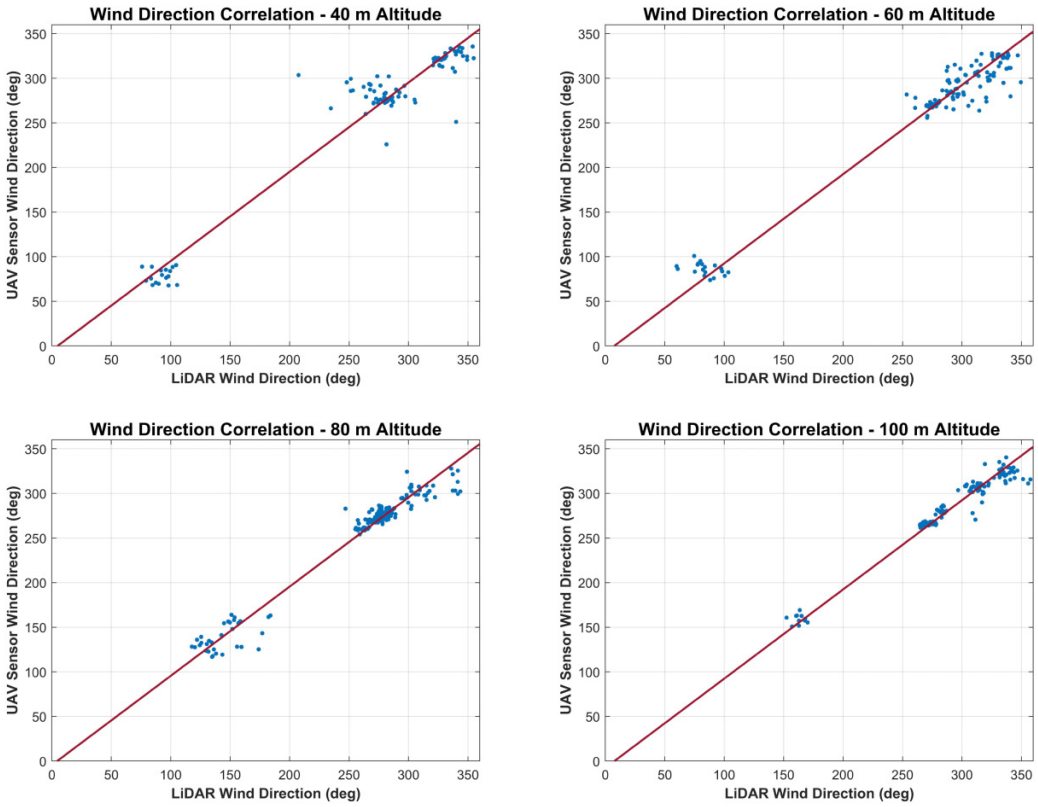

Data set	Model	No. of Data Points	R^2	RMSE (°)
40 m	$\theta_{UAV} = \theta_{LID} - 4.84$	105	0.937	20.96
60 m	$\theta_{UAV} = \theta_{LID} - 7.57$	134	0.957	15.44
80 m	$\theta_{UAV} = \theta_{LID} - 4.5$	176	0.960	11.34
100 m	$\theta_{UAV} = \theta_{LID} - 7.69$	158	0.949	9.46

Fig. 10. Hexacopter RPAS-mounted ultrasonic wind sensor to LiDAR wind direction delta with respect to ZX 300 LiDAR wind speed readings.

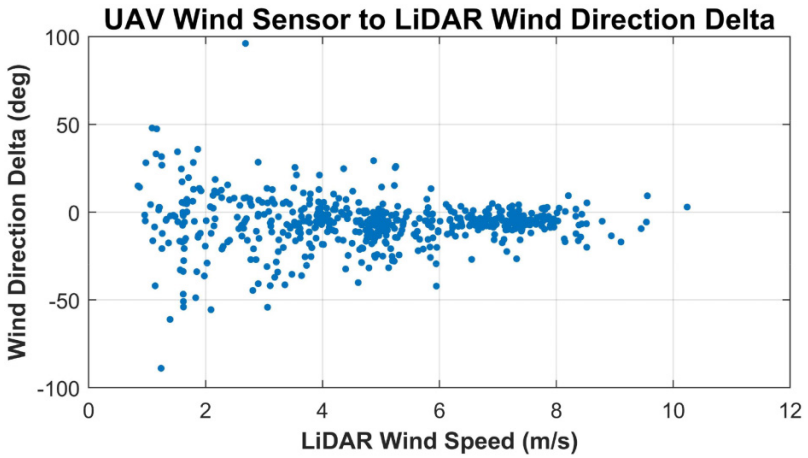

Fig. 11. Wind rose plots for flights conducted at an altitude of 5 m above ground at the Qormi sheltered site. Wind direction readings are with respect to the hexacopter RPAS heading.

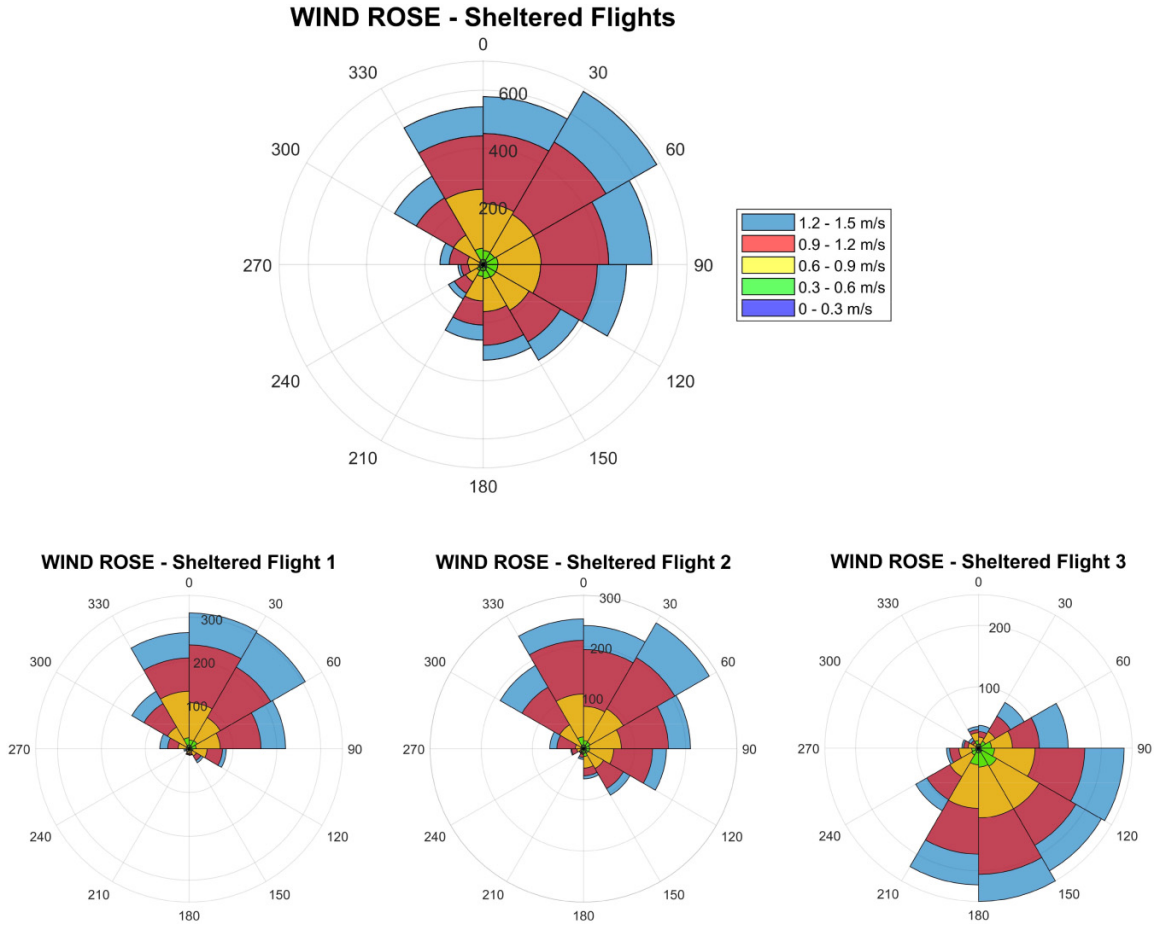

Table 1. Mean recorded wind speed for hexacopter RPAS flights in a sheltered location.

Test number	Mean wind speed (m/s)	Standard deviation (m/s)
1	0.984	0.325
2	0.981	0.336
3	1.109	0.505
Combined	1.029	0.408

5.1. Wind speed

The wind speed correlation results presented in Section 4 for the wind speed readings of the LiDAR unit and the hexacopter RPAS-mounted ultrasonic wind sensor indicate that the latter sensor's readings generally differ from the LiDAR wind speed measurements by a positive offset of 1 m/s. The regression line's gradient for the full data set across all flight altitudes was found to be 1.01 (Fig. 6). It was also observed that a consistent regression line gradient close to unity and an offset of 1 m/s were present for the wind speed data segregated by RPAS operational altitude (Fig. 7), indicating that the offset of 1 m/s does not change with increasing wind speed.

The wind speed offset observed may be caused by the different topography features at the two wind measurement points. Nonetheless, potentially it may also have been caused by the incident horizontal wind disturbing the inflow field of the RPAS rotors at the wind sensor level above the RPAS's centre hub, causing the flow to skew in the wind direction. This may have resulted in the mounted wind sensor measuring a higher horizontal wind speed than the actual atmospheric wind speed, as witnessed in previous studies (Palomaki et al. 2017; Shimura et al. 2018). The obtained results therefore further justify a proper investigation into the source of the 1 m/s offset to establish whether this was a topographically induced offset, an RPAS rotor airflow-induced offset, or potentially a combination of these two causes.

An attempt to establish the cause of this offset was made during this study by running sheltered location tests under both airborne and tied-down conditions in which the atmospheric wind speed was minimal. Due to the limited control

Fig. 12. Plan view of the hexacopter RPAS showing the bearing of each motor in relation to the front (nose) of the aircraft and its respective direction of rotation.

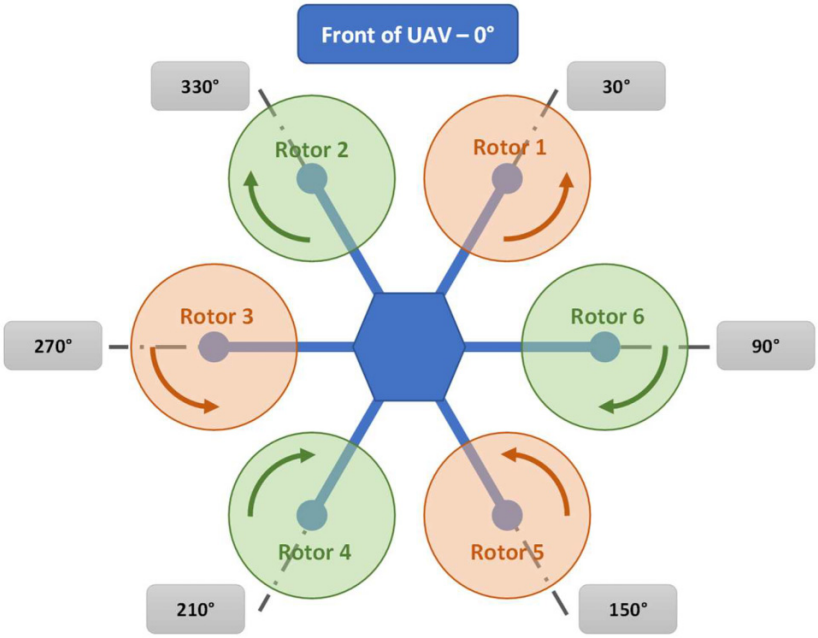

Fig. 13. Wind rose plots for two 3-min interval recordings of wind conditions during Test 3 (left) and Test 5 (right) of the tied-down test sequence for the hexacopter RPAS. Wind direction readings are with respect to the hexacopter RPAS heading.

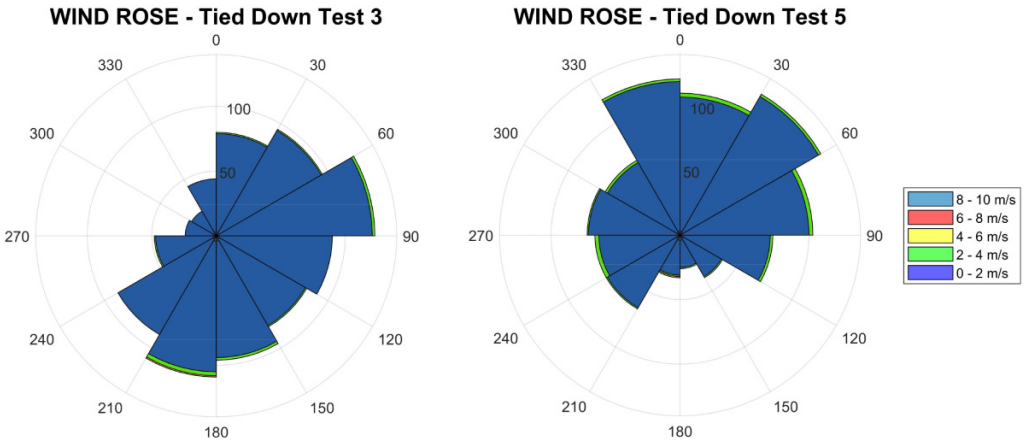

on the environment in which these tests were carried out, the cause of the wind speed offset could not be established with substantial certainty. However, the results for these tests presented in Section 4 do confirm that the rotor-induced flow does contribute to the offset.

5.2. Wind direction

The wind speed data analysis was followed by a similar analysis of the wind direction data detailed in Section 4. To analyse the relationship, it was deemed suitable to use a Cartesian plot thereby plotting the RPAS-mounted wind sensor measurements on the *y*-axis against the reference LiDAR wind measurements on the *x*-axis. A perfect correlation would yield a linear regression line having a gradient of unity and a *y*-intercept of zero. Although the data values fall in the range 0°–360°, this is a circular data range and it therefore transpires that the offset at the 0° and 360° positions should be equal. This was achieved by fixing the gradient of the fitted regression line at unity.

It should also be noted that the LiDAR unit was installed on the rooftop of an RO plant. Consequently, the unit was placed on top of a concrete structure which also contained a reinforcing steel mesh. Furthermore, the hall beneath the unit housed high voltage power transformer units required to power the RO plant, potentially generating significant magnetic fields. This could potentially lead to anomalies in the compass readings of the LiDAR unit, and to a lesser extent the compass readings of the RPAS-mounted instruments.

Fig. 14. Wind rose plots for hexacopter RPAS tied-down tests with all rotors powered up (Test 1) and with rotor 3 (Test 2) and rotors 3 and 4 (Test 4) disconnected. Wind direction readings are with respect to the hexacopter RPAS heading.

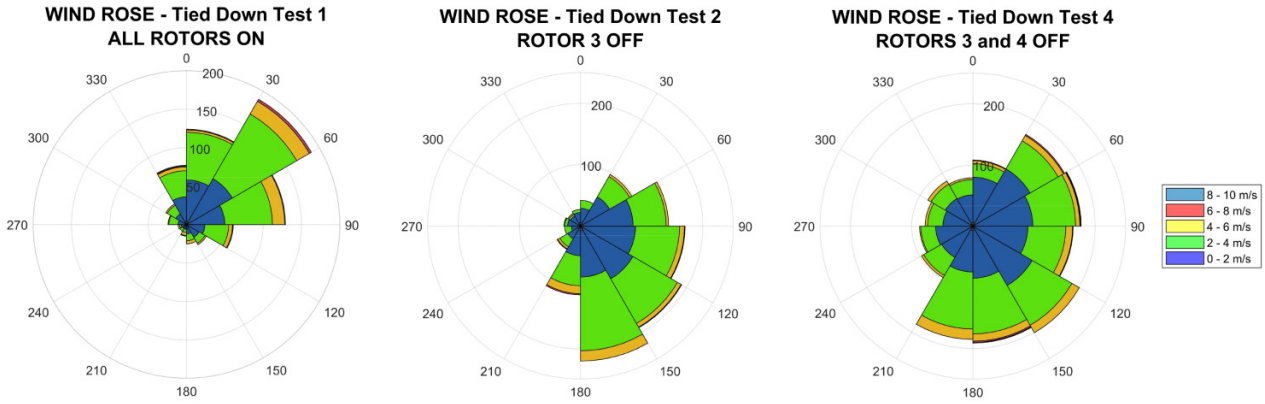

Table 2. Mean recorded wind speed during the hexacopter RPAS tied-down testing phase.

Test number	Flight setup	Mean wind speed (m/s)	Standard deviation (m/s)
1	All Rotors ON	2.350	1.271
2	Rotor 3 OFF	2.027	1.127
3	All Rotors OFF	0.474	0.446
4	Rotors 3 and 4 OFF	1.944	1.176
5	All Rotors OFF	0.506	0.527

Notwithstanding the possible electromagnetic environment, the data indicate a relatively strong correlation between the two sensing instruments.

The correlation for wind direction readings between the two instruments based on the Cartesian plot shown in Fig. 8, resulted in a negative wind direction offset of 6.16° for the ultrasonic sensor wind direction reading with respect to the LiDAR wind direction measurement. The offsets for the wind data segregated by flight altitude (Fig. 9), fall within a relatively tight angular range of less than 3°, more specifically between −4.84° and −7.69°. This indicates a reliable wind direction reading, which is further reinforced by the high R^2 values which exceed 0.93 for each of the wind direction correlation studies. Two main factors that may have significantly contributed to this offset could be a slightly altered wind profile from the LiDAR's measurement cone to the RPAS hovering site, as well as any minor misalignment in the mounting references of the two instruments. A third cause that may also have a minor influence on the resulting offset may be the difference in localized electromagnetic fields due to the electrical plant at the LiDAR installation site. The resulting offset may potentially be a combination of the above factors with each providing a minor contribution to the overall offset.

It was also observed that when incident wind speeds were in the lower magnitude range, a wider discrepancy was noticed in the wind direction readings between LiDAR and ultrasonic wind sensor readings (Fig. 10). This phenomenon was, to some extent expected, as lower wind speed conditions tend to give rise to relatively more independent localized wind eddy currents. These easily differ between the different measurement locations of the RPAS position at hover and the LiDAR measuring cone.

5.3. Sheltered test flights and tied-down testing

Having established that the wind speed data between the two sensors showed a 1 m/s offset, it was interesting to establish whether there may have been any particular RPAS-induced signature wind profile contributing towards this wind measurement offset. Should this have been the case, such signature wind profiles could be established for the various operating conditions of the RPAS and the various rotor speed profiles of the RPAS. This would enable the superimposing of such profiles onto the wind readings from the open field tests to further enhance the accuracy of the open field wind measurements. The purpose of conducting sheltered location RPAS flights as well as the tied-down tests was to identify whether such signature wind profiles were indeed present.

The recorded average wind speed measurements for the sheltered set of flights were very consistent with an overall average of 1.03 m/s and falling within a very tight range of magnitudes between 0.98 and 1.11 m/s (Table 1). Although this could very well be partially or completely caused by an incident wind at the time of the flights, it is also equivalent to the correlation offset between the RPAS's onboard sensor and the LiDAR wind speed measurements. Furthermore, the wind rose plots shown in Fig. 11, for the wind data during the airborne sheltered location flights, indicate a relatively wide wind direction spread, both within each flight

and across flights, with a relatively consistent wind speed spread in all wind directions. It should also be noted that the three airborne sheltered location flights were conducted within a tight 50-min window; a limited timeframe for the open field atmospheric wind conditions to change significantly between flights.

When the hexacopter RPAS was operated under tied-down conditions, the RPAS flight controller continued to demand close to maximum thrust (85% pulse width modulation duty cycle). Under these conditions, as the battery voltage drops so too does the revolutions per minute (rpm) of the RPAS's rotors, making testing under these conditions more challenging due to diminishing rpm. Nonetheless, it was evident that a significantly lower wind speed was measured during the sheltered location flights than when tests were run under outdoor tied-down conditions. This suggests that although the RPAS was set up with the rotor hubs at 1.2 m above the ground, the proximity of the ground influenced the wind speeds measured. Unfortunately, elevating the RPAS further during the outdoor testing would have exposed the wind sensor to stronger incident atmospheric wind currents, defying the scope of the tied-down tests, which was primarily to independently measure the effect of the RPAS's rotors on the wind sensor measurements.

A substantially noticeable difference in the average recorded wind speeds between the sheltered location flights' data sets and the tied-down tests exists, with an average recorded wind speed of 1.03 m/s for the former and an average recorded wind speed of 2.35 m/s for the tied-down test with all rotors running at full power. The recorded background average wind speed was of approximately 0.5 m/s, as evidenced in Table 2 by the average wind speeds for the two powered down tests. Although this substantial difference could have been caused by the proximity of the RPAS to the ground during tied-down testing, it should also be highlighted that the tied-down tests were run with rotors spinning at an average 5740 rpm, whilst the sheltered location flights were run with rotors spinning at an average 4560 rpm which was just enough to maintain the hexacopter RPAS in a stable hover.

Another particular observation is that although for both the sheltered location flights and the tied-down test with all rotors powered-up there is an appreciable number of occurrences in most of the direction sectors, a higher occurrence of incident wind was found in the 30°–60° relative wind direction sectors. Although this could possibly be an indication of a particular RPAS signature wind profile, this warrants a more extensive study focusing specifically on establishing any such signature wind profiles, as further outlined in Section 6.

6. Conclusions and further research

This paper validated wind measurements from a hexacopter RPAS-mounted ultrasonic sensor against data from a ground-based LiDAR unit. The following are the main conclusions drawn from this study.

1. Very good correlation was obtained between the wind speed data from the ultrasonic sensor and the LiDAR unit readings for all flight test altitudes. However, a positive offset of 1 m/s was identified. This offset remained approximately constant across all wind speeds and for all flight altitudes and may have partially resulted from the flow field induced by the six RPAS rotors.
2. The wind direction readings measured by the RPAS-mounted ultrasonic wind sensor were also well correlated to the LiDAR wind direction readings with a negative offset of 6.16°. The observed offset may have resulted from minor misalignments in the mounting references of the two instruments, as well as a potentially slightly different wind profile between measurement locations.

The consistently very good correlation observed across all operational hover altitudes between the RPAS-based ultrasonic wind sensor readings and LiDAR unit wind measurements demonstrates the potential for using the RPAS as an instrument for wind monitoring applications at high altitudes without the need for deploying expensive instrument platforms, albeit of a time-limited nature.

6.1. Recommendations for further research

The open field data collection flights highlighted the importance of maximizing the RPAS's flight endurance to enable the collection of wind data over an extended time window, or at a location further afield from the RPAS launch site. It is also evident that using the open field scenario for research purposes comes with its inherent challenges, as it is a relatively uncontrolled environment and hence very stochastic in nature. Isolating individual factors which potentially have an adverse effect on the RPAS-based wind sensor measurements is difficult to achieve in such uncontrolled environments. For a better understanding of the effects of individual factors on the onboard wind sensor measurements it is suggested that for data collection under no wind conditions, measurements are taken in an adequately sized indoor location. Untethered RPAS indoor flight tests would undoubtedly entail the use of alternative stabilizing systems, other than a GPS unit, such as stereo vision-based navigation or the use of laser range finders; stabilizing technologies necessary for the RPAS to maintain an autonomous stable hover even when subjected to minor external disturbances. Tied-down testing should be conducted with the RPAS fixed to an elevated structure at a substantial altitude above the ground to eliminate "ground effect" phenomena. For the purposes of establishing potential RPAS signature wind profiles when operating under different wind conditions, further testing may be carried out in the controlled environment of a suitably sized wind tunnel for a range of simulated wind speeds.

Article information

History dates

Received: 28 June 2022
Accepted: 20 December 2022
Version of record online: 2 March 2023

Data availability
Data generated or analysed during this study are not available due to such data being utilized for further studies which are intended for publication at a later date.

Author information

Author ORCIDs
Leo Scicluna https://orcid.org/0000-0003-0152-8416
Tonio Sant https://orcid.org/0000-0003-3957-1030
Robert N. Farrugia https://orcid.org/0000-0002-2919-4190

Competing interests
The authors declare there are no competing interests.

Funding information
The research work disclosed in this publication is funded by the ENDEAVOUR Scholarship Scheme (Malta). The scholarship is partly financed by the European Union – European Social Fund (ESF) under Operational Programme II – Cohesion Policy 2014 – 2020, "Investing in human capital to create more opportunities and promote the wellbeing of society".
The ZephIR ZX 300 LiDAR unit used in this study was purchased through the European Regional Development Fund (Grant No.: ERDF 335: Solar Research Lab), partially financed by the European Union.

References

Abichandani, P., Lobo, D., Ford, G., Bucci, D., and Kam, M. 2020. Wind measurement and simulation techniques in multi-rotor small unmanned aerial vehicles. IEEE Access, **8**: 54910–54927. doi:10.1109/ACCESS.2020.2977693.

Aerialtronics. 2020. Drone solutions for wind turbine inspection. [online]. Available from https://www.aerialtronics.com/en/applications/drones-for-wind-turbine-inspection#intro [accessed 25 November 2020].

Amukele, T., Ness, P.M., Tobian, A.A., Boyd, J., and Street, J. 2017. Drone transportation of blood products. Transfusion, **57**(3): 582–588. doi:10.1111/trf.13900. PMID: 27861967.

Anemoment LLC. 2018. TriSonica™ Mini wind and weather sensor. [online]. Available from https://anemoment.com/features/#trisonica-mini [accessed 10 November 2018].

CNBC. 2020. August 31 [online]. Available from https://www.cnbc.com/2020/08/31/amazon-prime-now-drone-delivery-fleet-gets-faa-approval.html [accessed 12 November 2020].

DHL. 2020. DHL's Parcelcopter: changing shipping forever. [online]. Available from https://discover.dhl.com/business/business-ethics/parcelcopter-drone-technology [accessed 20 October 2020].

DJI. 2015. DJI E800 Tuned Propulsion System. User Manual. [online]. Available from http://dl.djicdn.com/downloads/e800/en/E800_User_Manual_v1.0_en.pdf [accessed 17 June 2018].

DJI. 2017. N3 User Manual. [online]. Available from http://dl.djicdn.com/downloads/N3/20170825/N3_User_Manual_En_v1.4.pdf [accessed 30 July 2018].

Drummond, C.D., Harley, M.D., Turner, I.L., Matheen, A.N., and Glamore, W.C. 2015. UAV applications to coastal engineering. ; Australasian Coasts & Ports Conference, Aukland.

Eschmann, C.W., Kuo, C.-h., Kuo, C.-M., and Boller, C. 2012. Unmanned aircraft systems for remote building inspection and monitoring. ; 6th European Workshop on Structural Health Monitoring.

Estrada, M.A., and Ndomab, A. 2019. The uses of unmanned aerial vehicles - UAV's - (or drones) in social logistic: natural disasters response and humanitarian relief aid. Procedia Comput. Sci. **149**: 375–383. doi:10.1016/j.procs.2019.01.151.

Farrugia, R.N., and Sant, T. 2011. Wied Rini II–a five year wind survey at Malta. Wind Eng. **35**(4): 419–432. doi:10.1260/0309-524X.35.4.419.

Farrugia, R.N., and Sant, T. 2016. A wind resource assessment at Aħrax Point: a node for central Mediterranean offshore wind resource evaluation. Wind Eng. **40**(5): 438–446. doi:10.1177/0309524X16660019.

FedEx Newsroom. 2019. October 18.[online]. Available from https://newsroom.fedex.com/newsroom/wing-drone-deliveries-take-flight-in-first-of-its-kind-trial-with-fedex/ [accessed 10 November 2020].

FT Technologies. 2019. FT205. [online]. Available from https://fttechnologies.com/wind-sensors/lightweight/ft205/ [accessed 14 October 2019].

Galdies, C. 2011. The climate of Malta: statistics, trends and analysis 1951–2010. National Statistics Office, Valletta, Malta.

Gonzalez-Rocha, J., De Wekker, S.F., Ross, R.S., and Woosley, C.A. 2020. Wind profiling in the lower atmosphere from Wind-induced perturbations to multirotor UAS. Sensors, **20**: 1341. doi:10.3390. PMID: 32121450.

Hallermann, N., and Morgenthal, G. 2013. Unmanned aerial vehicles (UAV) for the assessment of existing structures, IABSE Symposium, Kolata.

Iberdrola. 2020. Inspections using drones. [online]. Available from https://www.iberdrola.com/innovation/drones-wind-farms [accessed 25 November 2020].

InterMet Systems, Inc. 2020. iMet-XQ2 UAV Sensor. [online]. Available from https://www.intermetsystems.com/products/imet-xq2-uav-sensor [accessed 14 July 2020].

Marino, M., Fisher, A., Clothier, R., Watkins, S., Prudden, S., and Leung, C.S. 2015. September. An evaluation of multi-rotor unmanned aircraft as flying wind sensors. Int. J. Micro Air Veh. **7**(3): 285–299. doi:10.1260/1756-8293.7.3.285.

Meier, K., Hann, R., Skaloud, J., and Garreau, A. 2022. Wind estimation with multirotor UAVs. Atmosphere, **13**: 551. doi:10.3390/atmos13040551.

National Oceanic and Atmospheric Administration. 2020. Magnetic field calculators. [online]. National Oceanic and Atmospheric Administration (NOAA). Available from https://www.ngdc.noaa.gov/geomag/calculators/magcalc.shtml [accessed July 2020].

Nolan, P.J., Pinto, J., González-Rocha, J., Jensen, A., Vezzi, C.N., Bailey, S.C., and Schmale, D.G. 2018. Coordinated unmanned aircraft system (UAS) and ground-based weather measurements to predict lagrangian coherent structures (LCSs). Sensors, **18**(12): 4448. doi:10.3390/s18124448. PMID: 30558335.

Palomaki, R.T., Rose, N.T., van den Bossche, M., Sherman, T.J., and De Wekker, S.F. 2017. Wind estimation in the lower atmosphere using multirotor aircraft. J. Atmos. Ocean. Technol. **34**(5): 1183–1191. doi:10.1175/JTECH-D-16-0177.1.

Prudden, S., Fisher, A., Marino, M., Mohamed, A., Watkins, S., and Wild, G. 2018. Measuring wind with small unmanned Aircraft systems. J. Wind Eng. Ind. Aerodyn. **176**: 197–210. doi:10.1016/j.jweia.2018.03.029.

Read, B. 2017. Life-saving drones. [online]. Royal Aeronautical Society.Available from https://www.aerosociety.com/news/life-saving-drones/ [accessed 15 October 2020].

Shimura, T., Inoue, M., Tsujimoto, H., Sasaki, K., and Iguchi, M. 2018. Estimation of wind vector profile using a hexarotor unmanned aerial vehicle and its application to meteorological observation up to 1000 m above surface. J. Atmos. Ocean. Technol. **35**: 1621–1631. doi:10.1175/JTECH-D-17-0186.1.

Tarot-Rc. 2020. Tarot FY680. [online]. Available from https://tarot-rc.com/fy680-six-axis-vehicle-rack-pure-carbon-tube-version-tl68b01-p2562583.html [accessed 10 December 2020].

Thielicke, W., Hubert, W., Muller, U., Eggert, M., and Wilhelm, P. 2021. Towards accurate and practical drone-based wind measurements with an ultrasonic anemometer. Atmos. Meas. Tech. **14**(2): 1303–1318. doi:10.5194/amt-14-1303-2021.

Tyutyundzhiev, N., Lovchinov, K., Martínez-Moreno, F., Leloux, J., and Narvarte, L. 2015. Advanced PV modules inspection using multirotor UAV. 31st European Photovoltaic Solar Energy Conference and Exhibition, Hamburg. pp. 2077–2081. doi:10.4229/EUPVSEC20152015-5BV.1.8.

Willis, D.J., Niezrecki, C., Kuchma, D., Hines, E., Arwade, S.R., Barthelmie, R.J., and Rotea, M. 2018. Wind energy research: State-of-the-art and future research directions. Renew. Energ. **125**: 133–154. doi:10.1016/j.renene.2018.02.049.

Wolf, C.A., Hardis, R.P., Woodrum, S.D., Galan, R.S., Wichelt, H.S., Metzger, M.C., and de Wekker, S.F.J. 2017. Wind data collection techniques on a multi-rotor platform. Systems and Information Engineering Design Symposium (SIEDS). IEEE, Charlottesville, VA. pp. 32–37. doi:10.1109/SIEDS.2017.7937739.

Xiang, G., Hardy, A., Rajeh, M., and Venuthurupalli, L. 2016. Design of the life-ring drone delivery system for rip current rescue. IEEE Systems and Information Engineering Design Symposium (SIEDS). IEEE, Charlottesville, VA. pp. 181–186. doi:10.1109/SIEDS.2016.7489295.

ZXLidars. 2020. ZX 300 (formerly ZephIR 300) onshore wind Lidar. [online]. Available from https://www.zxlidars.com/wind-lidars/zx-300/ [accessed 5 October 2020].